

## Automated identification of 3D lung CT image orientation

Hanung Adi Nugroho\*, Rizki Nurfauzi and Eka Legya Frannita

Department of Electrical and Information Engineering, Universitas Gadjah Mada, Indonesia

Received 30 October 2019

Revised 14 January 2020

Accepted 14 January 2020

### Abstract

Computerized tomography (CT) is one of the major high-resolution imaging modalities. It is especially useful in the early detection of lung abnormalities. However, CT images are sometimes stored with names that do not always indicate the order of 3D images. Using “SliceLocation” and “InstanceNumber” in the CT header, CT image slices can be arranged into 3D form. However, the orientation of 3D images may still be reversed. The objective of the proposed method is to automatically determine the orientation of ordered 3D lung CT images by identifying the position of the trachea. The two features consisting of area difference and mean of roundness along several slices are extracted. The full dataset of LIDC-IDRI containing 10,010 3D lung CT images was evaluated to measure the performance of the proposed method. This proposed method achieves 99.97% accuracy. The proposed procedure can be very useful for development of computer aided detection or diagnosis of 3D lung CT images.

**Keywords:** Automated identification, CAD, Data preparation, 3D lung CT image orientation

### 1. Introduction

Non-invasive medical imaging is an effective procedure for screening abnormalities in the lungs, especially in lung nodules. Several imaging modalities, including X-ray imaging, computerized tomography (CT), magnetic resonance imaging (MRI), positron emission tomography (PET) and PET-CT, have been used in detecting lung cancer [1-2]. CT is a simpler and less expensive imaging modality compared to MRI and PET [1]. Moreover, computerized tomography (CT) is the most sensitive imaging modality for detecting small lung nodules, particularly in the developed helical multi-slice technology [3]. Recently, low-dose CT was applied for a monitoring program for at-risk groups such as smokers [4]. The National Lung Screening Trial (NLST) claimed that using Low Dose Computed Tomography (LDCT) allows a 10% reduce mortality over that using X-rays [5].

Fast-growing medical imaging technology has become a generator of much data to facilitate faster and more detailed clinical solutions. However, there are some limitations (e.g., low detail, fatigue, and expertise) when radiologists have to manually evaluate much medical checkup data [6-10]. One example of radiologist dependence on expertise is in LIDC-IDRI datasets. LIDC-IDRI is one of the largest lung CT image databases. It consists of ground truth (GT) of nodule segmentation and classification. Ground truth (GT) was blindly evaluated by four radiologists. However, only 34.7% of GT nodules were annotated by the four radiologists [10].

The use of computer-aided detection (CAD) is a solution to overcome human limitations. However, it should follow radiological rules to recognize abnormalities in the lungs in novel research [11-12].

There are some general processes to design CAD with image processing, such as data acquisition, preprocessing, lung segmentation, nodule detection, false positive reduction and classification. Data acquisition is an important process in designing CAD systems. Image preprocessing has been performed to improve both the interpretability and quality of original chest CT images. Lung segmentation aims to extract data from the lungs while eliminating artifacts, bronchi, tracheae, fat, muscles and ribs. Improving accuracy, precision and decreased computational complexity depend on the quality of lung segmentation [13]. Some methods such as thresholding, shape-based methods, edge-based methods, morphological methods [1, 14] and combined methods [15-16] have been applied to segment the lungs.

CT images are stored in sliced (2D) images, especially with an axial alignment. Studies of field of 3D lung CT images are created from 2D images (slices) [17-20]. The stored CT data with a dicom extension in the LIDC-IDRI dataset is labelled with a random name which does not allow assembly of 3D forms. “SliceLocation” [16, 21] and “InstanceNumber” [22] are parameters related to IDs number that are stored in the header of CT images for so that 3D arrangement can be made from 2D slices. However, neither of these parameters guarantee that the 3D order has uniform

**Table 1** The image scale type distribution of the 1,010 3D lung CT images

Type of image scale	Intercept values	The number of patient IDs	The number of slices
HU scale	0	67	7,807
CT scale	-1000	69	20,277
	-1024	874	214,632
<b>Total</b>		<b>1,010</b>	<b>242,716</b>

**Table 2** Manufacturer distribution of 1,010 3D lung CT images

Manufacturer	The number of patient IDs	The number of slices
GE	669	159,867
Philips	74	22,027
SIEMENS	201	53,148
TOSHIBA	66	7,674
<b>Total</b>	<b>1,010</b>	<b>242,716</b>

orientation. Hence, top and bottom orientations of the 3D image may be randomly reversed [23].

There are several studies that need 3D lung CT images with the uniform orientation as input data. In [23], the area, circularity and air filled regions were features used to find the seed point for extracting trachea in 2D. The system assumed that the 3D lung CT image was of reversed order if the seed point was not found in the top region. However, the details of these rules are not well defined. In [24], the projected component labeling in each slice was employed to find abnormalities in the lung area growth. These abnormalities indicated that the lung areas were connected to each other in 2D form. Uniform orientation of data was required to find the lung fusion location. However, identification of 3D lung CT image orientation is not stated in data preparation. Many data cannot be processed due to this problem. Another similar case was reported by [25]. A 2D Hough transform along the axial plane was applied to detect the tracheal region. The location of the region was in the top region. Therefore, the 3D lung CT image with uniform orientation must be determined at the beginning of the process. Ordering of 3D lung CT images was done using numbers from the CT image header only. However, the IDs and even the error of the reversed order are not well stated.

In short, true problems are formulated based on the aforementioned studies. First, there are no performance reports of identification 3D lung CT image orientation ordered from slices arranged using two common IDs. Second, the identification of 3D lung CT image orientation has never before been studied using image processing. Therefore, the objective of this study is to identify the orientation of 3D lung CT images. Moreover, detection of both the apex of the lung and trachea in both of the sides (top and bottom regions) is a novel aspect of this study. Comparison of the proposed method with the two IDs commonly used is conducted to show the effectiveness of the method. This study evaluated the full LIDC-IDRI database.

## 2. Materials and methods

### 2.1 Data

The LIDC-IDRI public database [26] includes 1,010 3D lung CT images covering 1,398 cases with 244,330 2D axial images having a size of 124 GB. Each LIDC-IDRI folder contains two types of CT images, the main and the secondary data. The main data consist of 2D image sequences that can be arranged into 3D form. The secondary data are in the form of digital roentgen (CR/DX). Only the main data were used

in this study. They consist of 1,010 3D lung CT images (242,716 slices).

There are two scales in CT images, Hounsfield units (HU) and CT scales. Images stored in one of these scales can be identified using the *intercept* value stored in the CT image header. The conversion between these scales is given by Eq. 1 [27]. *Pixel value* is an intensity value in the CT scale. *Slope* is a parameter that is stored in the CT image header. The distribution of CT scale and manufacturer types with slice thickness characteristics in the LIDC-IDRI database are shown in Table 1 and Table 2, respectively.

$$HU = (Pixel\ value \times Slope) + Intercept \quad (1)$$

### 2.2 The proposed method

There are four steps proposed in the identification of 3D lung CT image orientation. The four steps are data preprocessing, lungs and trachea extraction, feature extraction in the suspected trachea slices, and the top and bottom CT identification.

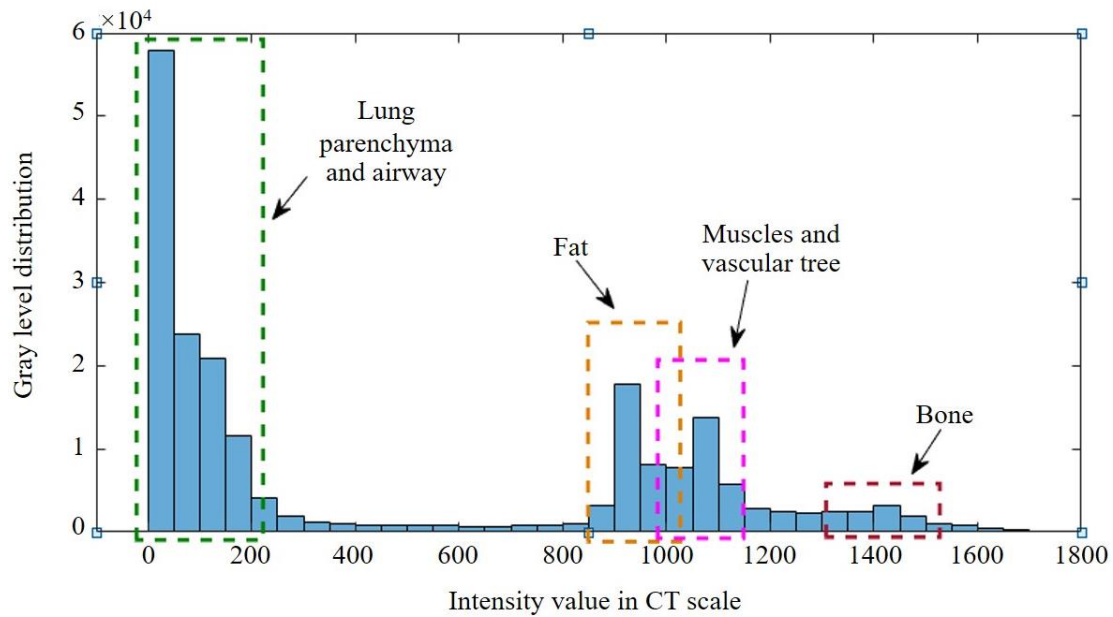
#### 2.2.1 Data preprocessing

Using “seriesUIDs” from a CT image header, 2D CT images can be arranged into a 3D CT image group. “SliceLocation” and “InstanceNumber” are two IDs stored in a header. The IDs allow a user to order the slices to form a 3D CT image.

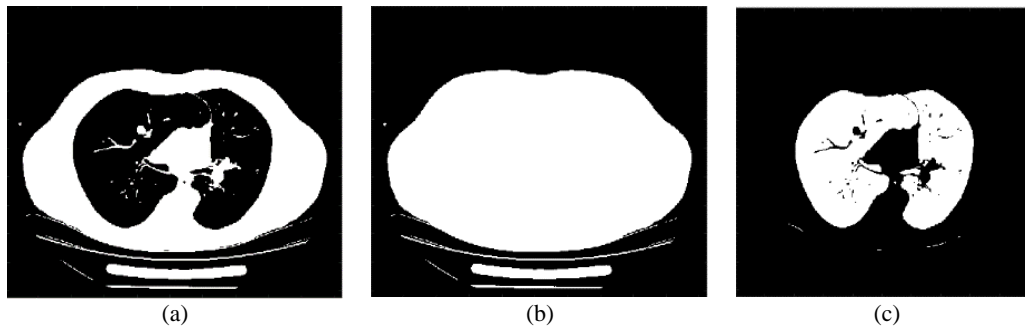
#### 2.2.2 Lung and trachea extraction

One of the ways to identify the top or the bottom of the 3D lung CT image orientation is to find the location of the trachea. Most areas of the lungs and trachea are filled with air, which in CT images appears with low intensity. To extract the lung and trachea area, the threshold value is considered. The quality of segmentation result depends on the selected threshold value.

A histogram of a regular lung CT image is shown in Figure 1. Determination of an optimum threshold value is crucial. The lungs and trachea regions have different intensities from other areas. Otsu thresholding is applied to find the optimum threshold value [28]. The result of the Otsu operation is a segmented image. The background is set for the lower intensity areas and foreground depicts a higher intensity area. Figure 1 is a histogram of a lung CT image, where the lung has low intensity. On the contrary, fat, muscles, the vascular tree and bone (vertebra, rib, and



**Figure 1** An example of intensity distribution of a lung CT image slice in CT scale.



**Figure 2** The lungs and trachea extraction in 2D processing: (a) result of Otsu thresholding applied on the chest, (b) result of morphological filling holes and (c) absolute value of subtraction of a from b.

sternum) have high intensities. Determination of an optimum threshold value between two contrasted peaks of low (lung) and high (fat, muscles, and bone) intensity is needed to extract the lungs.

Rough lung areas are extracted by adopting the method of [23]. To avoid more time consuming calculations [23], fuzzy c-mean is replaced by Otsu thresholding. The goal of lung extraction is to eliminate external artifacts of the patient's body. Accurate lung extraction based only the thresholding method is not an easy task for several reasons. First, the bed-mat where the patient lies and the patient's body are in close proximity. They have similar intensities in CT images. Second, partial volume effects caused by limited resolution of the imaging system are more difficult to analyze [15]. Third, the airway is an organ that is close to the lungs and requires an improved method to separate it.

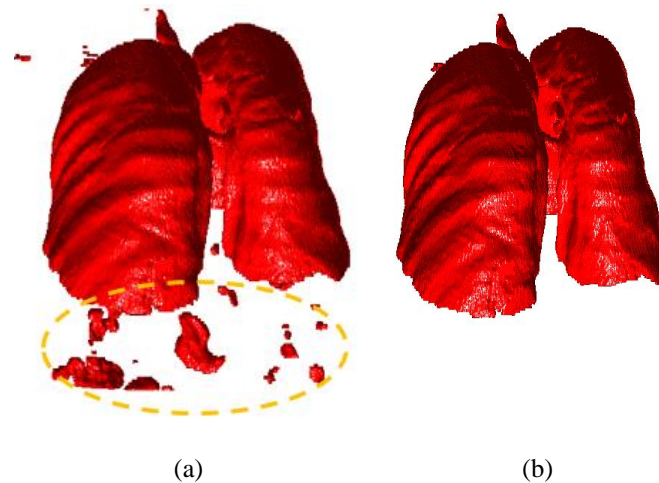
Otsu thresholding aims to find a threshold value while the sum of foreground and background spreads is a minimum value. After applying a thresholding method as shown in Figure 2 (a), 2D hole filling [29] is employed two times to locate the thorax, as shown in Figure 2 (b) and eliminate airways. The lungs are extracted by subtraction of the data in Figure 2(b) from Figure 2(a) as shown in Figure 2(c) and Figure 3(a). In the yellow enclosed area in Figure 3(a), the unwanted organ at the diaphragm is still seen. Finding the

largest connected component in 3D is done to eliminate the unwanted organ, as shown in Figure 3(b).

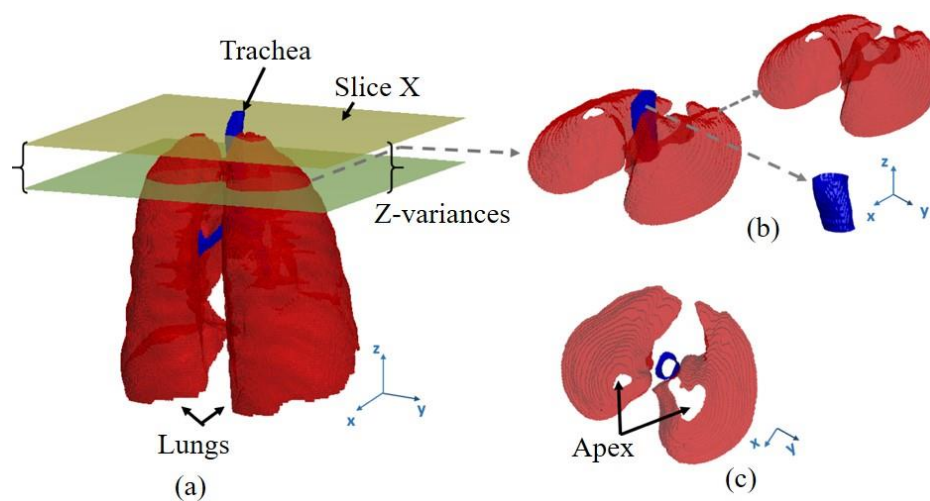
### 2.2.3 Feature extraction on a suspected tracheal slice

The novelty of this study is in the upper region of the lung to determine the 3D orientation of a lung in a CT image. Normally, after applying lung extraction, three regions remain, the two lungs and the trachea. The trachea has a more regular shape and greater homogeneity in area for several slices (in the range of Z-variance) compared to the lungs as shown in Figure 4(a). The trachea is covered by cartilage, which has a high circularity value in 2D and a regular shape in 3D compared to the lungs as shown in Figure 4(b). Figure 4(c) shows that the upper region of 3D lung CT image has three regions, the trachea in blue color and two lung apices in white. The two apices and a trachea area in 2D axial image have similar circularity and area. However, several areas in the bottom of the lung (diaphragm) have similarities to the three objects described before. To avoid the misidentification of the 3D lung CT image orientation due to these similarities, several methods are proposed as follows.

The first is an initial slice detection containing the suspected trachea and apex. The initial slice is called slice X, as shown in Figure 4(a). The detection process is started by



**Figure 3** Unwanted organ elimination in 3D processing: (a) before and (b) after perform organ elimination process.



**Figure 4** The difference shape and circularity between the lungs and trachea in several slices: (a) all slices in the lungs, (b) trachea and lung part on the z-variance slices, and (c) shown in axial plane.

finding the main regions (a trachea and two lung apex areas) in each slice from the upper to the lower sections. To prevent misdetection due to small unwanted organs in the diaphragm (as assumed when the 3D lung CT image is in an inverted orientation), the main areas are selected when each area has more than 1,000 pixels. Furthermore, to prevent misdetection of the two lung apices, one of the main areas should have a size of more than five times the main area (the minimum of suspected lung area).

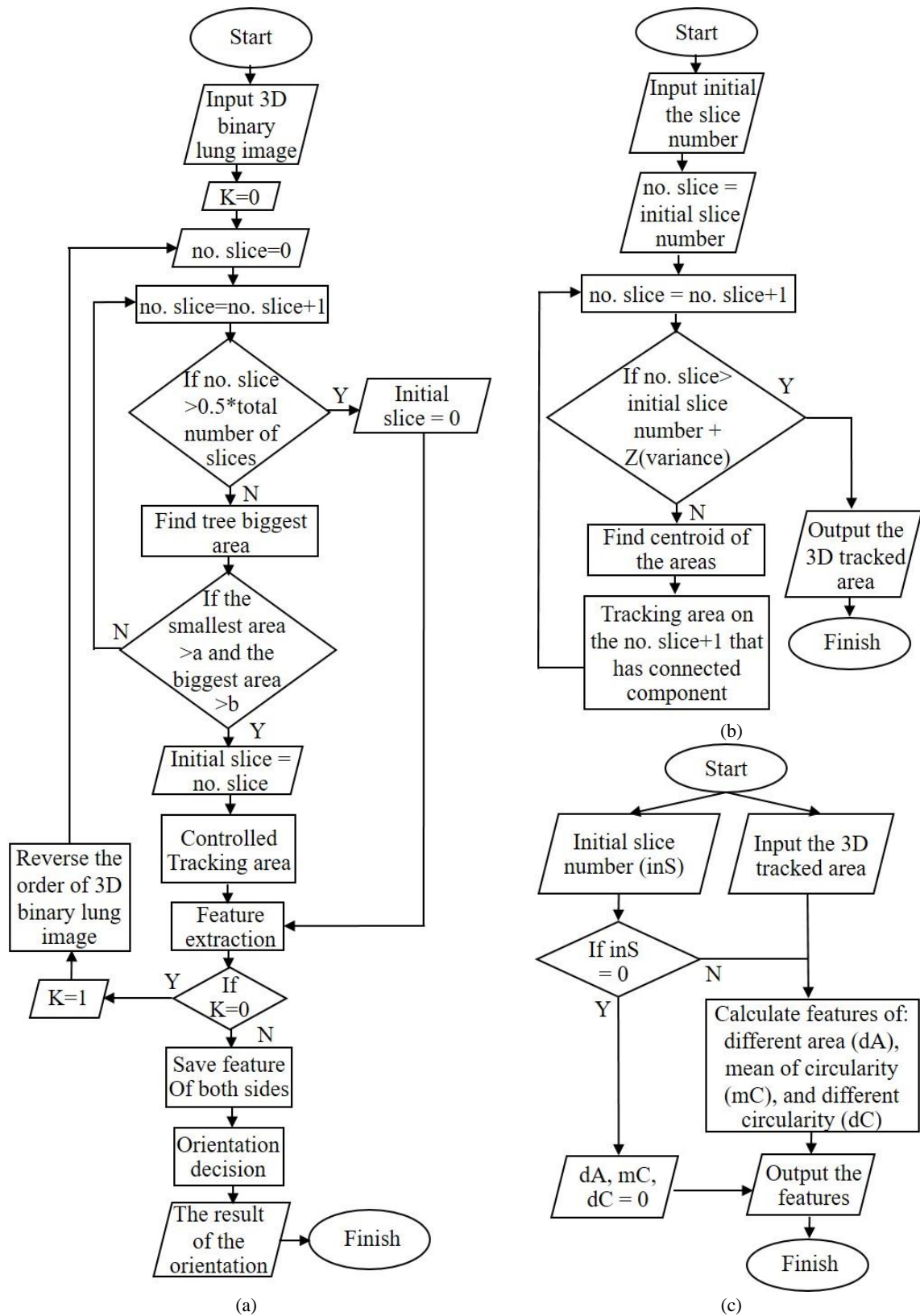
The second is feature extraction on the three main regions in Z-variance. The features are centroids, roundness and areas. The features are stored as temporary values. The centroid feature is used to track the connected area in the next slice. After conducting the tracking process through several slices, the process is continued by calculating the differences in area and the mean of roundness of features in the limited slices (Z-variance).

Different area features are applied to distinguish the trachea region from the two apex regions. The segmented area of the lower lung position tends to be greater than that of the higher lung position. On the contrary, the trachea area tends to have no significant changes. The centroid, roundness and area were calculated by [30]. Figure 5 presents a flowchart of the proposed method up to this stage. The a and b variables are defined as 1,000 pixels and 5,000 pixels.

#### 2.2.4 Identifying the top and bottom CT

The aim of this step is to determine the 3D lung CT image orientation by considering the extracted features of both orientations. There are three features, the mean of circularity (mC), mean of the differential circularity (dC) and mean of the differential area (dA). Limited slices (Z-variance) has variation of six up to 20 slices with an interval of two. From three areas (the two lungs and the trachea), the proposed method selects the highest value for each feature.

The extracted features of several slices in Z-variance are analyzed to find the location tendency (the top and the bottom). The maximum of the average of circularity values (maxmC), one minus the minimum of the average of the differential areas (maxdA) and one minus the minimum of the average of the differential circularity (maxdC) of each region (two areas of the right and left lungs as well as the tracheal area) are collected as candidate values. The final feature values are chosen by finding the maximum of each feature in all regions. To identify the top and the bottom of 3D lung CT images, the proposed method compares the final feature values on both of sides.

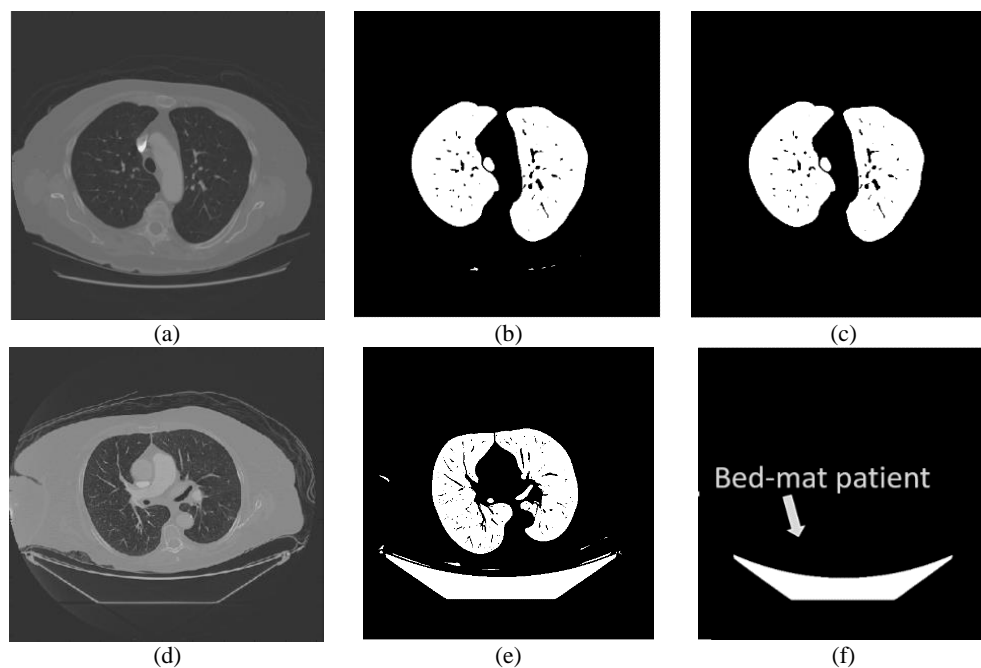


**Figure 5** A flowchart of all stages until feature extraction, (a) the general stage, (b) controlled tracking of area, and (c) feature extraction.

2.3 Testing dataset

Evaluation of a purposed scheme used 1,010 3D lung CT images from the LIDC-IDRI database. While the process

finds an error, the proposed method continues to the next dataset and notes a temporal variable to determine how many errors occurred. The performance is validated by accuracy. Accuracy is calculated by Eq. 2 as:



**Figure 6** Lung extraction results: (a-c) proper extraction and (d-f) improper extraction.

**Table 3** The result in each slice variation (Z-variances)

The number of analyzed slices (z-variances)	correct	miss	Accuracy (%)
6	1005	3	<b>99.7</b>
8	1005	3	<b>99.7</b>
10	1005	3	<b>99.7</b>
12	1004	4	99.6
14	1003	5	99.5
16	1004	4	99.6
18	1001	7	99.3
20	1001	7	99.3

$$accuracy = \frac{a \text{ number of correctly identified}}{a \text{ number of all data points}} \times 100 \quad (2)$$

### 3. Results and discussion

The objective of this study is to identify the orientation of 3D lung CT image ordered using “SliceLocation” or “InstanceNumber” stored in CT metadata. Locating the trachea is one of the ways to identify the top and the bottom location in the 3D lung CT images. A trachea has a high roundness value with small difference in area in serial slices. There were only two data sources that are not suitable to segment by the proposed method. The problem occurs because bed mats of patients are detected in the 3D lung CT images with larger areas than the lungs. Since the method selects the largest area, the system eliminates the lungs and leaves the bed mat. The segmented bed mat is shown in Figure 6 (a-b). Therefore, the remaining data that are available to identify the orientation of 3D lung CT images consist of 1,008 images.

From these 1,008 datasets, the 3D lung CT images are ordered using “SliceLocation” [16, 21] and “InstanceNumber” [22] with orientation identification accuracies of 71.9% and 95.6%, respectively. The results of orientation identification using fully automated image

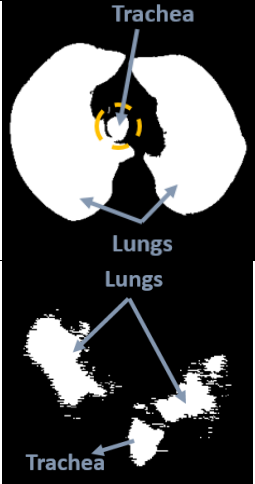

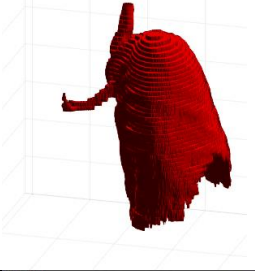

processing are reported in Table 3. The highest accuracy achieved is 99.7%, which is obtained in the range of six until ten of the Z-variance. Therefore, referring to Table 4, the best performance orientation identification is achieved by the proposed method. The most common of misidentification occurs in three dataset of 3D lung CT images, as illustrated in Table 5. The ordered data are 83, 662 and 953. They are caused by detection of only one part of a lung and with irregularly shaped lungs and trachea. Since only a part of lung is detected, the proposed method automatically identifies this detected result as the bottom orientation. The same treatment is conducted in irregularly shaped trachea due to presence of noise.

There are nine misidentified orientations identified. They are caused by four types of uncommon lung shapes, as shown in Table 4. The first uncommon shape is the area where the lungs and trachea are connected. The ordered data are 203, 482, 426 and 490. However, these cases only occur with a high Z-variance. The second uncommon shape has much noise. The ordered data are 662 and 786. This noise affects the results of segmentation. The system cannot identify the lungs and trachea since the necessary information is not in the rules. The third problem is when only a part of the lungs is segmented. This case affects three data in all of Z-variances. The last is caused by broken data. In 727 of ordered data, the slice order is broken. Broken data leads to

**Table 4** Comparison results of orientation detection process

Accuracy (%)	Only using IDs		Proposed method
	SliceLocation [16, 21]	InstanceNumber [22]	
	71.9%	95.6%	99.7%

**Table 5** Misidentification of 3D lung CT image

No	Type	LIDC	slice	Images
1	Connected with lung	0189 0484 0417 0944	24 24 20 25	
2	Noise	0658 0785	4 17	
3	Only one lung	0067 0957	- -	
4	Broken dicom file	0734	237	

inaccurate 3D lung reconstruction where only half of 3D lung area remains. Therefore, misidentified orientation only appears in high of Z-variances that contain a broken slice.

**4. Conclusions**

Finding the correct orientation of lung 3D CT images is an important issue in computer-aided diagnosis (CAD). This analysis requires homogeneously oriented input. The current research is a pilot study that evaluated the full LIDC-IDRI database with 1,010 3D lung CT images. Two images are not available to extract the lungs. The remaining 1,008 3D lung CT images were used in our analysis. From the results, excellent performance is achieved in identifying the 3D orientation of lungs in CT images in the LIDC-IDRI database with an accuracy of 99.7%. This result indicates that the proposed method has potential for implementation as part of CAD in data preparation, particularly in identifying the orientation of 3D CT lung images.

**5. Acknowledgements**

The authors would like to acknowledge colleagues of Intelligent System Research Group in the Department of Electrical and Information Engineering, Faculty of Engineering, Universitas Gadjah Mada, for inspiring discussion and anonymous reviewers for their encouraging recommendations.

**6. References**

- [1] Bhavanishankar K, Sudhamani MV. Techniques for detection of solitary pulmonary nodules in human lung and their classifications - a survey. *Int J Cybern Inf.* 2015;4(1):27-40.
- [2] Conway J. Lung imaging — two dimensional gamma scintigraphy, SPECT, CT and PET. *Adv Drug Deliv Rev.* 2012;64(4):357-68.
- [3] Diederich S, Lentschig MG, Overbeck TR, Wormanns

- D, Heindel W. Detection of pulmonary nodules at spiral ct: comparison of maximum intensity projection sliding slabs and single-image reporting. *Eur Radiol*. 2001;11(8):1345-50.
- [4] Santos AM, de Carvalho Filho AO, Silva AC, de Paiva AC, Nunes RA, Gattass M. Automatic detection of small lung nodules in 3D CT data using gaussian mixture models, tsallis entropy and SVM. *Eng Appl Artif Intell*. 2014;36:27-39.
- [5] Dajac J, Kamdar J, Moats A, Nguyen B. To screen or not to screen: low dose computed tomography in comparison to chest radiography or usual care in reducing morbidity and mortality from lung cancer. *Cureus*. 2016;8(4):e589.
- [6] Kundel H, Revesz G. Lesion conspicuity, structured noise, and film reader error. *Am J Roentgenol*. 1976;126(6):1233-8.
- [7] Berbaum KS, Franken EA Jr, Dorfman DD, Rooholamini SA, Kathol MH, Barloon TJ, et al. Satisfaction of search in diagnostic radiology. *Invest Radiol*. 1990;25(2):133-40.
- [8] Renfrew DL, Franken EA, Berbaum KS, Weigelt FH, Abu-Yousef MM. Error in radiology: classification and lessons in 182 cases presented at a problem case conference. *Radiology*. 1992;183(1):145-50.
- [9] Petrick N, Sahiner B, Armato SG 3rd, Bert A, Correale L, Delsanto S, et al. Evaluation of computer-aided detection and diagnosis systems. *Med Phys*. 2013;40(8):087001.
- [10] McNitt-Gray MF, Armato SG 3rd, Meyer CR, Reeves AP, McLennan G, Pais RC, et al. The lung image database consortium (LIDC) data collection process for nodule detection and annotation. *Acad Radiol*. 2007;14(12):1464-74.
- [11] Valente IRS, Cortez PC, Neto EC, Soares JM, de Albuquerque VHC, Tavares JMRS. Automatic 3D pulmonary nodule detection in CT images: a survey. *Comput Methods Programs Biomed*. 2016;124:91-107.
- [12] Lederlin M, Revel MP, Khalil A, Ferretti G, Milleron B, Laurent F. Management strategy of pulmonary nodule in 2013. *Diagn Interv Imaging*. 2013;94(11):1081-94.
- [13] Zhang J, Xia Y, Cui H, Zhang Y. Pulmonary nodule detection in medical images: a survey. *Biomed Signal Process Contr*. 2018;43:138-47.
- [14] Buket B, Ko P, Özçam A, Kanik SD. Lung nodule detection in x-ray images: a new feature set. In: Lacković I, Vasic D, editors. 6th European Conference of the International Federation for Medical and Biological Engineering; 2014 Sep 7-11; Dubrovnik, Croatia. Switzerland: Springer; 2015. p. 150-5.
- [15] Shen S, Bui AAT, Cong J, Hsu W. An automated lung segmentation approach using bidirectional chain codes to improve nodule detection accuracy. *Comput Biol Med*. 2015;57:139-49.
- [16] Nurfauzi R, Nugroho HA, Ardiyanto I. Lung detection using adaptive border correction. 2017 3rd International Conference on Science and Technology - Computer (ICST); 2017 Jul 11-12; Yogyakarta, Indonesia. USA: IEEE; 2017. p. 57-60.
- [17] Nithila EE, Kumar SS. Automatic detection of solitary pulmonary nodules using swarm intelligence optimized neural networks on CT images. *Eng Sci Technol Int J*. 2017;20(3):1192-202.
- [18] De Nunzio G, Tommasi E, Agrusti A, Cataldo R, De Mitri I, Favetta M, et al. Automatic lung segmentation in CT images with accurate handling of the hilar region. *J Digit Imaging*. 2011;24(1):11-27.
- [19] Jimenez-Carretero D, Bermejo-Peláez D, Nardelli P, Fraga P, Fraile E, Estépar RSJ, et al. A graph-cut approach for pulmonary artery-vein segmentation in noncontrast CT images. *Med Image Anal*. 2019;52:144-59.
- [20] Filho PPR, da Silva Barros AC, Almeida JS, Rodrigues JPC, de Albuquerque VHC. A new effective and powerful medical image segmentation algorithm based on optimum path snakes. *Appl Soft Comput*. 2019;76:649-70.
- [21] Lampert TA, Stumpf A, Gacarski P. An empirical study into annotator agreement, ground truth estimation, and algorithm evaluation. *IEEE Trans Image Process*. 2016;25(6):2557-72.
- [22] Nurfauzi R, Nugroho HA, Ardiyanto I, Frannita EL. Autocorrection of lung boundary on 3D CT lung cancer images. *J King Saud Univ. - Comput Inf Sci*. In press 2019.
- [23] Zhou S, Cheng Y, Tamura S. Automated lung segmentation and smoothing techniques for inclusion of juxtapleural nodules and pulmonary vessels on chest CT images. *Biomed Signal Process Contr*. 2014;13:62-70.
- [24] Cid YD, Del Toro OAJ, Depeursinge A, Müller H. Efficient and fully automatic segmentation of the lungs in CT volumes. *CEUR Workshop Proceedings*. 2015;1390:31-5.
- [25] Mansoor A, Bagci U, Xu Z, Foster B, Olivier KN, Elinoff JM, et al. A generic approach to pathological lung segmentation. *IEEE Trans Med Imaging*. 2014;33(12):2293-310.
- [26] Armato SG, McLennan G, Bidaut L, McNitt-Gray MF, Meyer CR, Reeves AP, et al. The lung image database consortium (LIDC) and image database resource initiative (IDRI): a completed reference database of lung nodules on CT scans. *Med Phys*. 2011;38(2):915-31.
- [27] Moosavi Tayebi R, Wirza R, Sulaiman PS, Dimon MZ, Khalid F, Al-Surmi A, et al. 3D multimodal cardiac data reconstruction using angiography and computerized tomographic angiography registration. *J Cardiothorac Surg*. 2015;10:58.
- [28] Otsu N. A threshold selection method from gray-level histograms. *IEEE Trans Syst Man Cybern*. 1979;9(1):62-6.
- [29] Gonzalez RC, Woods RE. Digital image processing. 3<sup>rd</sup> Ed. New Jersey, USA: Prentice-Hall; 2006.
- [30] Gonzales RC, Wood RE. Digital image processing. 2<sup>nd</sup> Ed. New Jersey, USA: Prentice Hall; 2002.